Tropical cyclone genesis potential index in climate models

SUZANA J. CAMARGO[1]*, ADAM H. SOBEL[2],

ANTHONY G. BARNSTON[1], and KERRY A. EMANUEL[3]

[1] International Research Institute for Climate and Society,

Lamont Campus, Palisades, NY

[2] Department of Applied Physics and Applied Mathematics,

and Department of Earth and Environmental Sciences,

Columbia University, New York, NY

[3] Program in Atmospheres, Oceans and Climate,

Massachusetts Institute of Technology, Cambridge, MA

*Corresponding author: Dr. Suzana J. Camargo, IRI - Monell 225, 61 Route 9W, Palisades, NY 10964-8000. Phone: +1 845 680 4416, Fax: +1 845 680 4865, E-mail: suzana@iri.columbia.edu.

Abstract

The potential for tropical cyclogenesis in a given ocean basin during its active season has been represented by a genesis potential index (GPI) that contains several large-scale environmental variables demonstrated to relate to tropical cyclone (TC) genesis. Here we examine the ability of some of today's atmospheric climate models, forced with historical observed SST over a multidecadal hindcast period, to reproduce observed values and patterns of the GPI, as well as the expected implications for their TC number. The evaluation is done toward the goal of being able to rely on climate models to predict anomalies in TC behavior, including activity level and preferred location, on time-scales from interannual through multidecadal and longer. The effect of the horizontal resolution of a climate model on its GPI is explored.

The five analyzed models are found capable of reproducing the observed seasonal phasing of GPI in a given region, but most of them them have a higher GPI than observed. Additionally, each model has its own unique relationship between mean GPI and mean TC number. The interannual correlation of GPI and number of TCs in a given basin differs significantly among models.

Experiments using different horizontal resolutions of the ECHAM5 model indicate that as resolution is increased, model GPI also increases for many of the ocean basins during their peak TC seasons. Most of this increase is realized between resolution T42 and T63, with much smaller increases for further resolution increases up to T159. Increases in model GPI with increasing resolution implies a more favorable large-scale environment for model TC genesis.

1. Introduction

Tropical cyclone-like disturbances have long been found in in climate simulations (Manabe et al., 1970; Bengtsson et al., 1982, 1995; Tsutsui and Kasahara, 1996; Vitart et al., 1997, 1999; Camargo and Sobel, 2004). These disturbances have properties qualitatively similar to those of observed tropical cyclones, but due to the low resolution of most simulations (with a few exceptions, e.g., Oouchi et al. (2006); Yoshimura et al. (2006)), are much weaker in amplitude and larger in scale than observed tropical cyclones. Despite this deficiency, tropical cyclone (TC) activity has been examined in global climate models for various purposes. One purpose is understanding large-scale climate influences on TCs. This has been explored using low-resolution atmospheric (e.g. Wu and Lau, 1992; Vitart and Anderson, 2001; Camargo et al., 2005) and coupled atmospheric-ocean models (Matsuura et al., 1999, 2003; Yumoto et al., 2003; Vitart et al., 2003; Vitart, 2006). Given the large difference in space and time scales between TCs and climate variability, computing limitations require compromise of some kind, and this approach, in which deficiencies in the simulation of TCs are accepted in order to allow explicit simultaneous simulation of larger-scale climate variability, has been a reasonable strategy.

One issue of particular interest is the skill of global models in forecasting year-to-year variability of seasonal TC activity. While the relatively low resolution of most climate simulations renders them inadequate for forecasting individual cyclones' tracks and intensities, some climate models do have skill in forecasting seasonal TC activity (Bengtsson, 2001). Currently, experimental dynamical seasonal forecasts of TC activity are issued by the International Research Institute for

Climate and Society (IRI, 2006) and the European Center for Medium-Range Weather Forecasts (Vitart and Stockdale, 2001; Vitart et al., 2003; Vitart, 2006). The approach used in producing these experimental dynamical forecasts is to detect and track TC-like like structures in the climate models (atmospheric or coupled atmosphere-ocean models).

Another topic of much recent interest is the possible influence of global climate change on TC activity (Emanuel, 2005a; Webster et al., 2005; Landsea, 2005; Pielke Jr. et al., 2005; Emanuel, 2005b; Pielke Jr., 2005; Hoyos et al., 2006; Chan, 2006; Anthes et al., 2006; Pielke Jr. et al., 2006; Mann and Emanuel, 2006). As climate models are tools of central importance in predictions of climate change, it is natural to use them to investigate the influence of greenhouse gases on TC activity. This has been done in a number of studies, using a variety of approaches (Broccoli and Manabe, 1990; Ryan et al., 1992; Haarsma et al., 1993; Bengtsson et al., 1996; Royer et al., 1998; Druyan et al., 1999; Walsh and Ryan, 2000; Sugi et al., 2002; Walsh et al., 2004; Knutson and Tuleya, 2004; Walsh, 2004; Bengtsson et al., 2006; Chauvin et al., 2006). An approach that has been used in some studies (Bengtsson et al., 1996; Sugi et al., 2002; Chauvin et al., 2006, e.g) involves identifying and tracking the models' TC-like vortices, and asking how their numbers and intensities change over time as the larger-scale climate does. Due to the relatively poor representation of TC dynamics in low-resolution climate models, results from this approach can be provocative, but not entirely convincing. As yet there have been very few global simulations using very high-resolution models and which simulate realistic TCs (Yoshimura et al., 2006; Oouchi et al., 2006).

Another approach to analyzing the relationship between TCs and climate, for the purpose of

forecasting both seasonal to interannual variations and long term changes, involves analyzing simulated variations in the large-scale environment, focusing on those large-scale variables known to affect TC activity (Ryan et al., 1992; Watterson et al., 1995; Thorncroft and Pytharoulis, 2001). The strength of this approach is that the ability of climate models to simulate the large-scale climate, while somewhat flawed, is clearly superior to their ability to simulate TCs. This approach thus plays to the strength of the models. A complication is that a choice has to be made regarding which variables, or combinations of variables, should be analyzed, and how the results should be interpreted, given that our understanding of the mechanisms by which the large-scale environment influences TC activity is limited. Recently, McDonald et al. (2005) compared both approaches using one climate model to track model TCs and analyze two genesis parameters in current and future climates.

We focus here on climate models' simulations of factors influencing the number of TCs that occur in a given basin in a given year. This number is governed by the process of tropical cyclogenesis. While much is known about which factors influence genesis, a quantitative theory (such as exists at least in part for intensity, as described in Emanuel (1995)), is lacking. In the absence of such a theory, empirical methods are useful. Gray (1979) developed an index which was able to replicate key features of the seasonal and spatial variability of observed genesis using a handful of environmental parameters. In this study, we use an empirical index called the genesis potential index, broadly similar to that of Gray, to quantify the proclivity of the large-scale environment to TC genesis.

We examine both the environment for TC activity, as well as the simulated TC activity itself, in five different atmospheric climate models. We wish to ascertain both how well the models simulate the climatological environment for TC genesis (as represented by the genesis potential index), compared to that found in a reanalysis data set, as well as whether the statistics of the simulated TC-like disturbances bear relationships to their simulated environments similar to those between real TCs and theirs. Evaluating the ability of current climate models to reproduce the genesis potential index is a first step toward analyzing the models' performance in future climate scenarios as well as the representativeness of the genesis potential index in forecasting the interannual variability of seasonal TC activity.

In section 2 we describe the genesis potential index, the models and the data used in this study. In section 3 the genesis potential index climatology in the models is discussed, and in section 4 the TC activity in the models is analyzed and compared with the genesis potential index characteristics. The influence of horizontal resolution is discussed in Section 5. A discussion and some conclusions are given in Section 6.

2. Methodology

The genesis potential index (GPI) that we use was developed by Emanuel and Nolan (2004), motivated by the work of Gray (1979), and has been used by Nolan et al. (2006) and Camargo et al. (2006a). We compare the climatological GPI, as simulated by the five models, to their simulated TC activity. The latter is obtained by detecting and tracking cyclone-like structures in the model

as described by Camargo and Zebiak (2002). A statistical analysis of various aspects of TC activity in three of these models was described in Camargo et al. (2005). The influence of horizontal resolution on the GPI will also be explored, by examining a single one of the models run at five different horizontal resolutions.

The GPI takes a set of environmental variables that, on physical grounds, reasonably might be expected to be important predictors of tropical cyclogenesis, and combines them into a single number, whose functional dependence on each variable is chosen to capture the spatial and temporal patterns of the genesis climatology and interannual variability in the observed record. In using the selected environmental variables, we avoid features that might be specific to the present climate, such as categorizations based on fixed thresholds. The set of predictors includes the potential intensity (Emanuel, 1986), relative humidity and absolute vorticity at various levels, and wind shear. The wind shear is defined as the magnitude of the vector difference between the horizontal winds at 850 and 200 hPa, as is often used in empirical studies of TC genesis and intensity change.

Emanuel and Nolan (2004) used monthly reanalysis data to relate the spatial and temporal variability of genesis to a limited number of environmental predictors, and developed the following index:

$$GP = \left|10^5\eta\right|^{3/2} \left(\frac{\mathcal{H}}{50}\right)^3 \left(\frac{V_{\rm pot}}{70}\right)^3 (1 + 0.1V_{shear})^{-2} ,$$

where η is the absolute vorticity at 850hPa in s^{-1}, $\mathcal{H}$ is the relative humidity at 700hPa in percent, $V_{\rm pot}$ is the potential intensity in ms^{-1}, and $V{\rm shear}$ is the magnitude of the vertical wind shear between 850hPa and 200hPa in ms^{-1}.

The technique to obtain potential intensity $V_{\rm pot}$ is a generalization of the one described in Bister and Emanuel (2002a) and takes into account dissipative heating (Bister and Emanuel, 1998), in addition to sea surface temperature (SST), sea level pressure (SLP), and atmospheric temperature and mixing ratio at various pressure levels. The climatological, or low-frequency, variability of the potential intensity was presented in Bister and Emanuel (2002a,b).

Although the GPI was developed by a statistical fitting procedure based only on the seasonal cycle and spatial variation of the mean genesis climatology of the reanalysis, composites of the GPI were developed for El Niño and La Niña years separately (Camargo et al., 2006b). The composite anomalies reproduce interannual variations in the observed frequency and location of genesis with some skill, for several different basins (Camargo et al., 2006b). This independent test shows that the index has some utility for understanding the influence of climate variations on TC activity.

To define and track TCs in the models, we use objective algorithms (Camargo and Zebiak, 2002) based in large part on prior studies (Vitart et al., 1997; Bengtsson et al., 1995). The algorithm has two parts. In the detection part, storms that meet environmental and duration criteria are identified. A model TC is identified when chosen dynamical and thermodynamical variables exceed thresholds based on observed tropical storm climatology. Most studies (Bengtsson et al., 1982; Vitart et al., 1997) use a single set of threshold criteria globally; however, these do not take into account model biases and deficiencies. We use basin- and model-dependent threshold criteria, based on each model's own climatology (Camargo and Zebiak, 2002). The second part is the tracking, in which the tracks are obtained from the vorticity centroid, defining the center of the TC

using relaxed criteria. The detection and tracking algorithms have been previously applied to regional climate models (Landman et al., 2005; Camargo et al., 2006c) and to several global climate models (Camargo and Zebiak, 2002; Camargo et al., 2005). The dynamics of model TC formation over the western North Pacific have also been explored using this tracking algorithm (Camargo and Sobel, 2004).

The models used in our analysis are three versions of the European Community-Hamburg models (ECHAM3.6, ECHAM4.5, ECHAM5), the National Center for Atmospheric Research (NCAR) Community Climate Model 3.6 (CCM3.6), and the NSIPP (NASA Seasonal to Interannual Prediction Project) atmospheric model. The first three models were developed at the Max-Planck Institute for Meteorology, Hamburg, Germany (Model User Support Group, 1992; Roeckner et al., 1996; Roeckner and Co-Authors, 2003), the fourth model at NCAR, Boulder, Colorado (Kiehl et al., 1998) and the last one at NASA/Goddard in Maryland, USA; (Suarez and Takacs, 1995). Output from all these models is currently available at IRI. The precise time periods of the simulations and number of ensemble members varies, as given in Table 1.

Here, the GPI of the five climate models and of the National Center for Environmental Prediction/National Center for Environmental Research (NCEP/NCAR) Reanalysis (Kalnay et al., 1996) is calculated using monthly mean data. The TCs in the models are also identified and tracked using either 6-hourly or daily data output from the models, depending on data availability.

The TC statistics are computed from the best-track datasets developed by the National Hurricane Center (for Atlantic and eastern Pacific) and Joint Typhoon Warning Center (for western

North Pacific and southern Hemisphere), respectively (JTWC, 2006; NHC, 2006). From the observed data sets, only TCs with tropical storm or hurricane/typhoon intensity are considered here, i.e. tropical depressions are not included.

3. Genesis potential index model climatology

In Fig. 1 the annual maximum of the monthly GPI climatology at each grid point is shown for the models and the reanalysis observations. All models capture the well known TC regions, appearing as maxima of the GPI. With the exception of ECHAM3 Fig. 1(a), all models have considerably higher values of the GPI than those in the reanalysis. Consequently, the regions conducive to TC genesis (by the standards appropriate for observations) appear much larger in all the models except ECHAM3. Because genesis in the models may bear a quite different relationship to the GPI, quantitatively, than in observations, this does not necessarily mean that genesis will actually occur more frequently or over a larger area in a given model than in observations.

The ECHAM4, ECHAM5 and NSIPP models have large values for the GPI in the western North Pacific, while the highest values in the Atlantic occur in the NSIPP model. ECHAM4, ECHAM5 and NSIPP are also the models having highest GPI values in the Southern Hemisphere. All models reproduce the movement of the regions of large GPI from the Northern to the Southern Hemisphere (not shown).

The annual cycle of the mean annual cycle of the GPI in four regions is shown in Fig. 2. The definitions of the basins, subbasins and their peak seasons are given in Table 2. The models

realistically simulate the basic timing of the TC activity in all four regions, although the month of the maximum does not always coincide with that of the observations. This is particularly true in the case of the North Indian Ocean, where there are two TC sub-seasons: pre- (AMJ) and post- (OND) Indian monsoon. Most models do capture this feature at least qualitatively, though the first peak occurs too early in the NSIPP model and is nearly entirely missed by the CCM. In most cases, the relative magnitudes of the GPI in the models and in the reanalysis are ordered consistently from one basin to the next, with, e.g., the reanalysis, ECHAM3, and CCM tending to have the smallest GPI and the NSIPP and ECHAM5 the largest. There are exceptions to this, such as the second peak in the North Indian basin being stronger in CCM than in NSIPP.

Table 3 shows, individually by basin, the interannual correlation between the seasonal GPI in the models and in the reanalysis for the peak season. Significant correlations occur in the Australian, western and eastern North Pacific, and Atlantic regions, for most models. In these regions and seasons, some of these same models had been found to have skill in simulating TC activity (see Tables 6 and 7 in Camargo et al. (2005)). However, some models that have minimally significant model vs. reanalysis GPI correlations for the North Indian Ocean, were found to have low simulation skill in model TC activity. Conversely, in the South Pacific region, where most models were found to have skill in simulating TC activity, significant model vs. reanalysis seasonal GPI correlations are absent.

By considering smaller regions or subbasins (defined in Table 2), the correlations of the GPI in the models and reanalysis increase noticeably in many subbasins (Table 4). This can be easily

understood in some regions, as in the case of the western North Pacific. In warm (cold) ENSO (El Niño-Southern Oscillation) events the TC genesis shifts to the southeast (northwest) (Wang and Chan, 2002), but changes in total basin genesis are minimal. There is no significant signal in the GPI for the whole basin, when the increase in one part of the basin is compensated by a decrease in the another part. When two smaller regions are considered, whose boundary takes into account these typical locational shifts, the mean GPI in each subbasin has a more clearly identifiable interannual signal and the interannual correlations are larger.

4. Model TC activity climatology

Fig. 3 shows the climatological annual total track density for the models and observations. The track density is obtained by counting the number of 6-hourly track positions of the TCs per 4° latitude and longitude per year, and in the case of the models, the ensemble mean is used. In the case of models with only daily output (CCM and NSIPP) the track density is multiplied by 4 to be consistent with the other models and observations.

The models' TC activity occurs in approximately the same locations as in observations (Fig. 3(f)), with model track density patterns differing somewhat from those of the observations and from one another. For instance, all models have too much near-equatorial TC activity. This may be a result of the models' low resolutions.

NSIPP (Fig. 3(d)) has little TC activity in the eastern Pacific and the North Atlantic. In observations, the track density has two strong maxima in the Northern Hemisphere: one in the eastern

and one in the western North Pacific. The models that most clearly reproduce these maxima are ECHAM4 and ECHAM5. In the Southern Hemisphere the track density maximum in the observations lies along a zonal band about 15 degrees south of the equator. In most models, the pattern in the Southern Hemisphere is less zonal, having a more oblique orientation in the southern Indian and southern Pacific Oceans, similar to the south Pacific convergence zone in the latter case.

Comparing Figs. 1 and 3, one notices that differences in GPI climatology between one model and another are not necessarily consistent with differences in the track density between the same two models. For instance, while the GPI climatology of the ECHAM3 (Fig. 1(a)) has the lowest values of all models, the same is not true of its track density (Fig. 3(a)). The NSIPP model has one of the highest values of the GPI in the North Atlantic (Fig. 1(d)), but very low TC activity in that region (Fig. 3(d)). Clearly, model-model differences in the simulated GPI in a specific region, or even for the global mean, need not have any consistent relationship to the corresponding differences in TC activity.

Let us compare in more detail the GPI and the number of TCs, by comparing the annual cycle of both quantities in the western North Pacific (Fig. 4) and the North Atlantic (Fig. 5). While in some cases there is a good match in the phasing of the annual cycle of TC activity and the mean GPI (e.g. Figs. 4(c), 4(e), 5(a)), in other cases the match is marginal or poor (e.g. Figs. 4(b), 4(d), 5(b), and 5(d)). Thus, in some cases the peak of the model TC activity in the model does not occur when the GPI in the model peaks, while in reanalysis observations the coincidence of the two quantities is close (see Figs. 4(f) and 5(f)), with number of TCs slightly lagging the genesis

potential in the Atlantic. Note that the GPI was developed by fitting the reanalysis data to describe the seasonal cycle and the spatial variation of the genesis location.

The relationship between the GPI and the number of TCs generated by a given model is further examined by looking at the scatter plot of the models' mean GPI and number of TCs (NTC) in the western North Pacific for the period of July to October for all years and ensemble members, shown in Fig. 6(a). Each point represents a single year and single ensemble member. The clustering of the different models in different parts of the plot indcates that there is not a consistent relationship, across models, between a model's western North Pacific mean GPI and its s western North Pacific mean NTC. Further, within any given model, there is not an immediately evident positive relationship between the GPI and NTC from one year or ensemble member to another. However, Fig. 6(b) shows a weak positive relationship between the mean GPI and NTC in the eastern part of the western North Pacific. As discussed above in the context of Table 2), when considering a smaller western north Pacific region that focuses a better defined SST-related interannual signal, a relationship between GPI and NTC is more clearly identified.

Next we examine the interannual correlations of the mean model GPI, during peak season, and the number of model TCs for the same season in individual basins and subbasins (as defined in Table 2. This relationship is extremely dependent on basin and model. The correlations between mean GPI and number of model TCs per basin during the peak season is given in Table 5. While the correlation of these two quantities in the Atlantic for ECHAM4 model is high and significant (0.77), in the western North Pacific it is much smaller, for the reason discussed above regarding

within-basin locational shifting of TC activity from year to year, and the related larger scale GPI-determining envirnomental fields, as a function of the ENSO state. While the total western north Pacific TC activity level does not have marked interannual variability, an ENSO influence is is clearly reflected in the subbasin activity levels, (e.g. Wang and Chan, 2002), the southeastern part having enhanced TC activity during El Niño. The GPI anomalies in the western North Pacific have a corresponding dipole of opposing anomaly values in ENSO years in the sub-regions defined by this shift (Camargo et al., 2006b). Accordingly, when the western North Pacific is divided into eastern and western subregions Table 6, the interannual correlation between the models' observed mean GPI and the observed number of TCs increases dramatically. Somewhat higher values of correlations for appropriately divided subregions are also found in most Southern Hemisphere subbasins. Note that because the ECHAM5 model has only 2 ensemble members (Table 1) its correlations are expected to be somewhat diminished.

It has been shown in previous studies that the skill of the models in simulating TC activity on a seasonal to interannual time-scale is model and basin dependent (Camargo et al., 2005). In some of the basins in which the models were found to have significant skill for number of TCs on seasonal time-scales, such as the eastern North Pacific and the Atlantic (see Tables 6 and 7 in Camargo et al. (2005)), correlations between the GPI and the number of TCs are positive and significant in the present study. In models that have problems producing TCs in some basins, with a mean number near zero (e.g. NSIPP in the Atlantic; see Table 2 in Camargo et al. (2005)), the relationship of the GPI with the number of TCs is less meaningful, and even a significant correlation should be

considered tentatively. Hence, in Table 6 an asterisk on a correlation coefficient indicates that the number of model TCs is zero for at least half of the years in the sample.

It is also of interest whether the seasonal GPI in the models could be used as a predictor of seasonal TC activity in observations. To evaluate that, we calculate the correlation of the model mean seasonal GPI with the observed number of TCs in the peak season for different regions (as defined in Table 2), shown in Tables 7 and 8. Again, the skill of the models is basin and model dependent, and in many basins higher skill is obtained when the smaller regions are considered. The models have skill in the Australian, South Pacific, western and eastern North Pacific and Atlantic basins (sometimes in just one of the subbasins). This implies that the GPI could be used to complement the dynamical forecasts in regions where tracking models' TC activity explicitly does not lead to significant skill, as in the case of the Bay of Bengal (in eastern North Indian Ocean) using the ECHAM4 model.

5. Influence of spatial resolution on the genesis potential index

It is well known that by increasing the horizontal resolution, the models' ability to reproduce TCs increases (Bengtsson et al., 1995). Given the strong control on TC dynamics known to be exerted by horizontal resolution, it may be natural to assume that it is this control on simulated TC dynamics that makes the statistics of TC activity so resolution-dependent. Here we explore whether some of this resolution dependence may be due to changes in the simulated environment, as represented by the simulated genesis potential.

The GPI was calculated for the ECHAM5 model at five different horizontal resolutions: T42, T63, T85, T106, and T159, as described in Table 1. In all cases the model was forced with observed SSTs for the period 1978-1999. For T42, T63, T85 and T106, there are 2 ensemble members, with different vertical resolutions: 19 and 31 levels, respectively. In the case of T63, the three additional ensemble members have vertical resolution of 19 levels, while for T159 there is only one ensemble member with vertical resolution of 31 levels. The cyclone (tropical and extratropical) activity of the ECHAM5 model was examined in Bengtsson et al. (2006), by tracking cyclones using the method described in (Hodges, 1994). Here, we showed the TC activity of the ECHAM5 with T42 horizontal resolution, computed using the method of Camargo and Zebiak (2002), in Figs. 3, 4 and 5.

The annual cycle of these increases in genesis potential are shown for four regions in Fig. 7, as a function of the horizontal resolution. In all cases, the minimum values of the mean GPI at the peak season occurs for the lowest resolution (T42). By increasing the horizontal resolution the GPI increases in specific areas, such as the North and South Atlantic, Northeast Pacific and in the Southern Hemisphere. The GPI in the Northwest Pacific and North Indian Ocean increases by smaller amounts. The most noticeable increase in the index occurs when resolution is increased from T42 to T63, with only small additional increases for T85, T106 and T159. In some cases though, there is also an appreciable increase going from T106 to T159.

These results imply that when the horizontal resolution of the model is increased, not only is there an improvement in the dynamics of the simulated TC-like disturbances, but the environmen-

tal conditions become more conducive to generation of TCs–at least in one model. Even if this result holds in other models, it is not immediately obvious that the environmental changes are for the better in terms of their impact on cyclone genesis and life cycle, since different models have different relationships between the simulated GPI and NTC. The lower portion of Table 7 reveals no systematic increase in correlation between model GPI and observed NTC in any of the basins, as wholes, when increasing the resolution in the ECHAM5 model. (A more sensitive examination might apply this analysis to correlations for the subbasins–to be done in a future study.) However, for basins in which the region conducive to genesis is relatively small in spatial extent, and which have negative biases in some models, such as the north Atlantic and eastern north Pacific, it is reasonable to speculate that increasing horizontal resolution may lead to improvement in the simulated TC climatology, due to both its effect on storm dynamics and on the environment.

6. Discussion and Conclusions

The genesis potential index (GPI) has been used to predict the potential for tropical cyclogenesis on the basis of several large-scale environmental variables known to contribute to tropical cyclone (TC) genesis. Here we examine the GPI, and its relationship with TC number, in several atmospheric climate models that are forced with historical observed SST as the lower boundary condition over a multidecadal hindcast period. These GPI vs. TC number relationships in the models are compared with those found in reanalysis observations in several ocean basins during their peak TC seasons. The motivation is to explore to what extent today's models are able to

reproduce the spatial and temporal variations of the GP index observed (using reanalysis data) in nature and to identify consequent effects on the models' abilities to predict the interannual or interdecadal variability, or a climate change-related trend, in the TC activity level. Because a lack of adequate horizontal spatial resolution is a known impediment to realistic reproduction of TCs in climate models, a range of spectral resolutions (from T42 to T159) is used for one of the models to investigate effects on the model GPIand TC activity level.

The models are found to reproduce quite well the reanalysis-observed phasing of the annual cycle of GPI in a given region. However, most of the models have a considerably higher GPI, overall, than that observed. It would be useful to know why the GPI tends to be higher in the models than in the reanalysis. Which of the four factors of the GPI might be contributing the most? A preliminary analysis of the fields of percentage difference between model and reanalysis, for each factor, by basin and model, indicates that the relative humidity contributes to the models' inflated GPI more than any other factor. This is particularly true for ECHAM4 and ECHAM5, whose GPI values are higher than the observed GPI by the greatest percentages. A caveat that should be kept in mind is that the relative humidity in the reanalysis is itself largely modeled, and may not represent reality perfectly.

Perhaps more importantly, the models have their own distinct, and widely differing, relationships between mean GPI and mean number of TCs. For example, in the Northern Hemisphere the ECHAM4 and NSIPP models have GP index within about 15 percent of one another for the June-November period, but ECHAM4 has roughly four times the number of TCs of NSIPP. This

strongly suggests that the large variations in the TC climatologies of the models are controlled more by variations in the dynamics of the model storms themselves than on variations in the simulated environments for genesis.

The interannual correlation of GPI and number of TCs differs significantly from one model to another, either falling short of, equaling, or in some cases even exceeding that found in the reanalysis observations for a given region during its active TC season. In some basins, where year-to-year variations in TC behavior involve mainly a shift in the location of TC genesis and track location within the basin rather than total basin-wide activity (e.g. in the west north Pacific in response to ENSO), the basin-wide average GPI and TC number are not expected to meaningfully reflect year-to-year changes in the environmental variables. In the western North Pacific, such locational signals are better reflected in the indices, and their interannual correlation becomes significant, when the basin is subdivided into western and eastern portions.

Experiments using different horizontal resolutions of the ECHAM5 model indicate that as horizontal resolution is increased in steps from T42 to T159, model GP index progressively increases by total amounts of roughly 15 to 50 percent, depending on ocean basin and season. Most of this increase is realized in stepping from T42 to T63, with only small further progressive increases up to T159. While a general increase in the correlation between model GPI and observed cyclone number was not achieved in whole ocean basins, the increases in GPI found when increasing the horizontal resolution implies a more favorable large-scale environment for TC genesis for higher resolution models, and, one would hope, greater responsiveness in terms of TC number.

Acknowledgements This work was support in part by NOAA through a block grant to the International Research Institute for Climate and Society.

References

Anthes, R., Corell, R., Holland, G., Hurrell, J., MacCracken, M., and Trenberth, K., Hurricanes and global warming – potential linkages and consequences, *Bull. Amer. Meteor. Soc.*, **87**, 623–628, 2006.

Bengtsson, L., Hurricane threats, *Science*, **293**, 440–441, 2001.

Bengtsson, L., Böttger, H., and Kanamitsu, M., Simulation of hurricane-type vortices in a general circulation model, *Tellus*, **34**, 440–457, 1982.

Bengtsson, L., Botzet, M., and Esch, M., Hurricane-type vortices in a general circulation model, *Tellus*, **47A**, 175–196, 1995.

Bengtsson, L., Botzet, M., and Esch, M., Will greenhouse gas-induced warming over the next 50 years lead to higher frequency and greater intensity of hurricanes?, *Tellus*, **48A**, 57–73, 1996.

Bengtsson, L., Hodges, K. I., and Roeckner, E., Storm tracks and climate change, *J. Climate*, accepted, 2006.

Bister, M. and Emanuel, K. A., Dissipative heating and hurricane intensity, *Meteor. Atm. Phys.*, **52**, 233–240, 1998.

Bister, M. and Emanuel, K. A., Low frequency variability of tropical cyclone potential intensity, 1, interannual to interdecadal variability, *J. Geophys. Res.*, **107**, 4801, doi:10.1029/2001JD000776, 2002a.

Bister, M. and Emanuel, K. A., Low frequency variability of tropical cyclone potential intensity, 2, climatology for 1982-1995, *J. Geophys. Res.*, **107**, 4621, doi:10.1029/2001JD000780, 2002b.

Broccoli, A. J. and Manabe, S., Can existing climate models be used to study anthropogenic changes in tropical cyclone climate?, *Geophys. Rev. Lett.*, **17**, 1917–1920, 1990.

Camargo, S. J. and Sobel, A. H., Formation of tropical storms in an atmospheric general circulation model, *Tellus A*, **56**, 56–67, 2004.

Camargo, S. J. and Zebiak, S. E., Improving the detection and tracking of tropical storms in atmospheric general circulation models, *Wea. Forecasting*, **17**, 1152–1162, 2002.

Camargo, S. J., Barnston, A. G., and Zebiak, S. E., A statistical assessment of tropical cyclones in atmospheric general circulation models, *Tellus*, **57A**, 589–604, 2005.

Camargo, S. J., Emanuel, K. A., and Sobel, A. H., Genesis potential index and ENSO in reanalysis and AGCMs, in *27th Conference on Hurricanes and Tropical Meteorology*, 15C.2, American Meteorological Society, Monterey, CA, 2006a.

Camargo, S. J., Emanuel, K. A., and Sobel, A. H., Use of a genesis potential index to diagnose ENSO effects on tropical cyclone genesis, *J. Climate*, submitted, available online at: http://iri.columbia.edu/cgi-bin/staff?scamargo, 2006b.

Camargo, S. J., Li, H., and Sun, L., Feasibility study for downscaling seasonal tropical cyclone activity using the NCEP regional spectral model, *Int. J. Clim.*, accepted, 2006c.

Chan, J. C. L., Comment on ”Changes in tropical cyclone number, duration, and intensity in a warming environment”, *Science*, **311**, 1713, 2006.

Chauvin, F., Royer, J.-F., and Déqué, M., Response of hurricane-type vortices to global warming as simulated by ARPEGE-Climat at high resolution, *Clim. Dyn.*, **27**, 377–399, doi: 10.1007/s00382-006-0135-7, 2006.

Druyan, L. M., Lonergan, P., and Eichler, T., A GCM investigation of global warming impacts relevant to tropical cyclone genesis, *Int. J. Climatol.*, **19**, 607–617, 1999.

Emanuel, K., Increasing destructiveness of tropical cyclones over the past 30 years, *Nature*, **436**, 686–688, doi:10.1038/nature03906, 2005a.

Emanuel, K., Emanuel replies, *Nature*, **438**, E13, doi:10.1038/nature04427, 2005b.

Emanuel, K. A., An air-sea interaction theory for tropical cyclones. Part I: Steady-state maintenance, *J. Atmos. Sci.*, **43**, 585–604, 1986.

Emanuel, K. A., Sensitivity of tropical cyclones to surface exchange coefficients and a revised steady-state model incorporating eye dynamics, *J. Atmos. Sci.*, **52**, 3969–3976, 1995.

Emanuel, K. A. and Nolan, D., Tropical cyclone activity and global climate, in *26th Conference on Hurricanes and Tropical Meteorology*, pp. 240–241, Amer. Meteor. Soc., Miami, FL, 2004.

Gray, W. M., *Meteorology over the tropical oceans*, chap. Hurricanes: Their formation, structure and likely role in the tropical circulation, pp. 155–218, Roy. Meteor. Soc., 1979.

Haarsma, R. J., Mitchell, J. F. B., and Senior, C. A., Tropical disturbances in a GCM, *Clim. Dyn.*, **8**, 247–257, 1993.

Hodges, K. I., A general method for tracking analysis and its application to meteorological data, *Mon. Wea. Rev.*, **122**, 2573–2586, 1994.

Hoyos, C. D., Agudelo, P. A., Webster, P. J., , and Curry, J. A., Deconvolution of the factors contributing to the increase in global hurricane intensity, *Science*, doi: 10.1126/science.1123560, 2006.

IRI, IRI (International Research Institute for Climate and Society) Tropical Cyclone Activity Experimental Dynamical Forecasts, available on line at: http://iri.columbia.edu/forecast/tc_fcst, 2006.

JTWC, JTWC (Joint Typhoon Warning Center) best track dataset, available online at https://metoc.npmoc.navy.mil/jtwc/best_tracks/, 2006.

Kalnay, E., Kanamitsu, M., Kistler, R., Collins, W., Deaven, D., Gandin, L., Iredell, M., Saha, S., White, G., Woollen, J., Zhu, Y., Chelliah, M., Ebisuzaki, W., Higgins, W., Janowiak, J., Mo, K., Ropelewski, C., Wang, J., Leetmaa, A., Reynolds, R., Jenne, R., and Joseph, D., The NCEP/NCAR 40-year reanalysis project, *Bull. Amer. Meteor. Soc.*, **77**, 437–441, 1996.

Kiehl, J. T., Hack, J. J., Bonan, G. B., Boville, B. A., Williamson, D. L., and Rasch, P. J., The national center for atmospheric research community climate model: Ccm3, *J. Climate*, **11**, 1131–1149, 1998.

Knutson, T. R. and Tuleya, R. E., Impact of CO_2-induced warming on simulated hurricane intensity and precipitation: Sensitivity to choice of climate model and convective parametrization, *J. Climate*, **17**, 3477–3495, 2004.

Landman, W. A., Seth, A., and Camargo, S. J., The effect of regional climate model domain choice on the simulation of tropical cyclone-like vortices in the southwestern indian ocean, *J. Climate*, **18**, 1263–1274, 2005.

Landsea, C. W., Hurricanes and global warming, *Nature*, **438**, E11–13, doi:10.1038/nature04477, 2005.

Manabe, S., Holloway, J. L., and Stone, H. M., Tropical circulation in a time-integration of a global model of the atmosphere, *J. Atmos. Sci.*, **27**, 580–613, 1970.

Mann, M. E. and Emanuel, K. A., Atlantic hurricane trends linked to climate change, *EOS*, **87**, 233,238,241, 2006.

Matsuura, T., Yumoto, M., Iizuka, S., and Kawamura, R., Typhoon and ENSO simulation using a high-resolution coupled GCM, *Geophys. Res. Lett.*, **26**, 1755–1758, 1999.

Matsuura, T., Yumoto, M., and Iizuka, S., A mechanism of interdecadal variability of tropical cyclone activity over the western North Pacific, *Clim. Dyn.*, **21**, 105–117, 2003.

McDonald, R. E., Bleaken, D. G., Cresswell, D. R., Pope, V. D., and Senior, C. A., Tropical storms: representation and diagnosis in climate models and the impacts of climate change, *Clim. Dyn.*, **25**, 19–36, 2005.

Model User Support Group, Echam3 - atmospheric general circulation model, Tech. Rep. 6, Das Deutshes Klimarechnenzentrum, Hamburg, Germany, 184pp., 1992.

NHC, NHC (National Hurricane Center) best track dataset, available online at http://www.nhc.noaa.gov, 2006.

Nolan, D. S., Rappin, E. D., and Emanuel, K. A., Could hurricanes form from random convection in a warmer world?, in *27th Conference on Hurricanes and Tropical Meteorology*, 1C.8, American Meteorological Society, Monterey, CA, 2006.

Oouchi, K., nd H. Yoshimura, J. Y., Mizuta, R., and Kusunoki, S., Tropical cyclone climatology in a global-warming climate as simulated in a 20km-mesh global atmospheric model: Frequency and wind intensity analyses, *J. Meteor. Soc. Japan*, **84**, 259–276, 2006.

Pielke Jr., R., Landsea, C., Mayfield, M., Laver, J., and Pasch, R., Reply to "Hurricanes and global warming potential linkages and consequences", *Bull. Amer. Meteor. Soc.*, **87**, 628–631, 2006.

Pielke Jr., R. A., Are there trends in hurricane destruction?, *Nature*, **438**, E11, doi:10.1038/04426, 2005.

Pielke Jr., R. A., Landsea, C., Mayfield, M., Laver, J., and Pasch, R., Hurricanes and global warming, *Bull. Amer. Meteor. Soc.*, **86**, 1571–1575, 2005.

Roeckner, E. and Co-Authors, The atmospheric general circulation model ECHAM5. Part I: Model description, Tech. rep., Max-Planck Institute for Meteorology, Hamburg, Germany, 127 pp., 2003.

Roeckner, E., Arpe, K., Bengtsson, L., Christoph, M., Claussen, M., Dümenil, L., Esch, M., Giorgetta, M., Schlese, U., and Schulzweida, U., The atmospheric general circulation model ECHAM-4: Model description and simulation of present-day climate, Tech. Rep. 218, Max-Planck Institute for Meteorology, Hamburg, Germany, 90 pp., 1996.

Royer, J.-F., Chauvin, F., Timbal, B., Araspin, P., and Grimal, D., A GCM study of the impact of greenhouse gas increase on the frequency of occurrence of tropical cyclone, *Climatic Change*, **38**, 307–343, 1998.

Ryan, B. F., Watterson, I. G., and Evans, J. L., Tropical cyclone frequencies inferred from Gray's yearly genesis parameter: Validation of GCM tropical climate, *Geophys. Res. Lett.*, **19**, 1831–1834, 1992.

Suarez, M. J. and Takacs, L. L., Documentation of the Aries/GEOS dynamical core Version 2, Technical Report Series on Global Modelling and Data Assimilation, NASA Technical Memorandum 104606 Vol. 5, Goddard Space Flight Center, Greenbelt, MD, USA, 58 pp., 1995.

Sugi, M., Noda, A., and Sato, N., Influence of global warming on tropical cyclone climatology: An experiment with the JMA global model, *J. Meteor. Soc. Japan*, **80**, 249–272, 2002.

Thorncroft, C. and Pytharoulis, I., A dynamical approach to seasonal prediction of Atlantic tropical cyclone activity, *Wea. Forecasting*, **16**, 725–734, 2001.

Tsutsui, J. I. and Kasahara, A., Simulated tropical cyclones using the National Center for Atmospheric Research community climate model, *J. Geophys. Res.*, **101**, 15 013–15 032, 1996.

Vitart, F., Seasonal forecasting of tropical storm frequency using a multi-model ensemble, *Q. J. R. Meteorol. Soc.*, **132**, 647–666, doi:10.1256/qj.05.65, 2006.

Vitart, F. and Anderson, J. L., Sensitivity of Atlantic tropical storm frequency to ENSO and interdecadal variability of SSTs in an ensemble of AGCM integrations, *J. Climate*, **14**, 533–545, 2001.

Vitart, F., Anderson, J. L., and Stern, W. F., Simulation of interannual variability of tropical storm frequency in an ensemble of GCM integrations, *J. Climate*, **10**, 745–760, 1997.

Vitart, F., Anderson, J. L., and Stern, W. F., Impact of large-scale circulation on tropical storm frequency, intensity and location, simulated by an ensemble of GCM integrations, *J. Climate*, **12**, 3237–3254, 1999.

Vitart, F., Anderson, D., and Stockdale, T., Seasonal forecasting of tropical cyclone landfall over Mozambique, *J. Climate*, **16**, 3932–3945, 2003.

Vitart, F. D. and Stockdale, T. N., Seasonal forecasting of tropical storms using coupled GCM integrations, *Mon. Wea. Rev.*, **129**, 2521–2537, 2001.

Walsh, K., Tropical cyclones and climate change: unresolved issues, *Clim. Res.*, **27**, 77–83, 2004.

Walsh, K. J. E. and Ryan, B. F., Tropical cyclone intensity increase near Australia as a result of climate change, *J. Climate*, **13**, 3029–3036, 2000.

Walsh, K. J. E., Nguyen, K. C., and McGregor, J. L., Fine-resolution regional climate model

simulations of the impact of climate change on tropical cyclones near Australia, *Clim. Dyn.*, **22**, 47–56, 2004.

Wang, B. and Chan, J. C. L., How strong ENSO events affect tropical storm activity over the western North Pacific, *J. Climate*, **15**, 1643–1658, 2002.

Watterson, I. G., Evans, J. L., and Ryan, B. F., Seasonal and interannual variability of tropical cyclogenesis: Diagnostics from large-scale fields, *J. Climate*, **8**, 3052–3066, 1995.

Webster, P. J., Holland, G. J., Curry, J. A., and Chang, H.-R., Changes in tropical cyclone number, duration, and intensity in a warming environment, *Science*, **309**, 1844–1846, 2005.

Wu, G. and Lau, N. C., A GCM simulation of the relationship between tropical storm formation and ENSO, *Mon. Wea. Rev.*, **120**, 958–977, 1992.

Yoshimura, J., Sugi, M., and Noda, A., Influence of greenhouse warming on tropical cyclone frequency, *J. Meteor. Soc. Japan*, **84**, 405–428, 2006.

Yumoto, M., Matsuura, T., and Iizuka, S., Interdecadal variability of tropical cyclone frequency over the western north pacific in a high-resolution atmosphere-ocean coupled GCM, *J. Meteor. Soc. Japan*, **81**, 1069–1086, 2003.

List of Figures

1 Annual maximum of monthly genesis potential index in the period 1961-2000: (a) ECHAM3, (b) CCM3, (c) ECHAM4, (d) NSIPP, (e) ECHAM5 (for 1978-1999, resolution T42), (f) NCEP reanalysis 33

2 Annual cycle of mean genesis potential index in the models and reanalysis observations in the (a) Western North Pacific, (b) North Atlantic, (c) North Indian and (d) South Indian basins, in the period 1950-2004, with the exception the ECHAM5 model (for 1978-1999, resolution T42). 34

3 Track density climatological annual total in the period 1961-2000: (a) ECHAM3, (b) CCM3, (c) ECHAM4, (d) NSIPP, (e) ECHAM5 (for 1978-1999, resolution T42), (f) observations. 35

4 Annual cycle of genesis potential (GP) index (blue bars - left scale), and number of tropical cyclones (NTC) in the western North Pacific for the period 1961-2000 in models: ECHAM3 (a), CCM3 (b), ECHAM4 (c), NSIPP (d), ECHAM5 (for 1978-1999, resolution T42) (e), NCEP reanalysis GP and observed NTC (f). 36

5 Annual cycle of genesis potential index (GPI) (blue bars - left scale), and number of tropical cyclones (NTC) in the w North Atlantic for the period 1961-2000 in models: ECHAM3 (a), CCM3 (b), ECHAM4 (c), NSIPP (d), ECHAM5 (for 1978-1999, resolution T42) (e), NCEP reanalysis GP and observed NTC (f). 37

6 Scatter plot of number of model tropical cyclones (NTC) and genesis potential index (GPI) in the western North Pacific (a) and the eastern part of the western North Pacific (b)in the period July to October. 38

7 Genesis potential index in the period 1978-1999 for the ECHAM5 model for 5 different horizontal resolutions (T42, T63, T85, T106 and T159) in the (a) Western North Pacific, (b) North Atlantic, (c) North Indian and (d) South Indian basins. . . 39

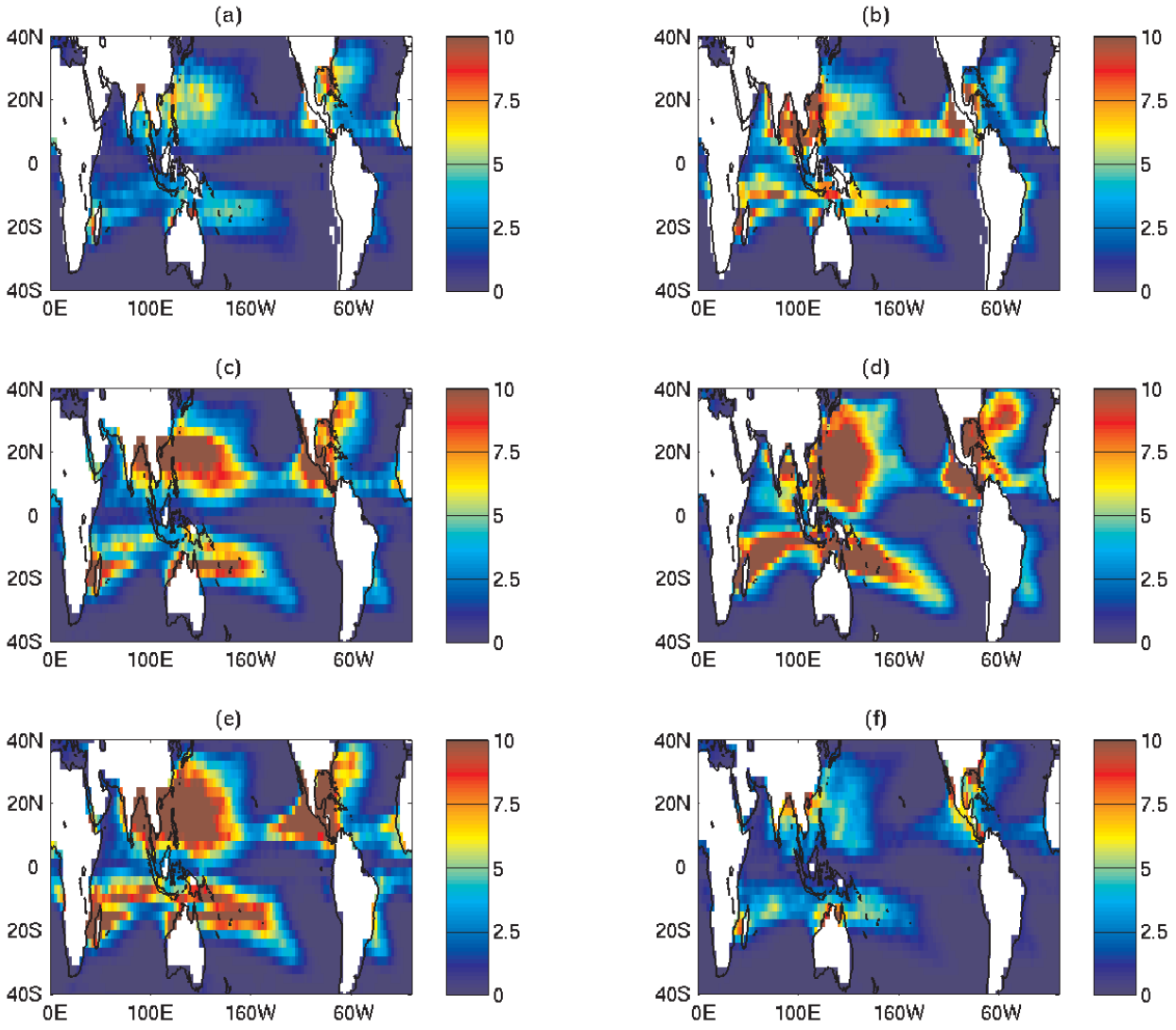

Figure 1: Annual maximum of monthly genesis potential index in the period 1961-2000: (a) ECHAM3, (b) CCM3, (c) ECHAM4, (d) NSIPP, (e) ECHAM5 (for 1978-1999, resolution T42), (f) NCEP reanalysis

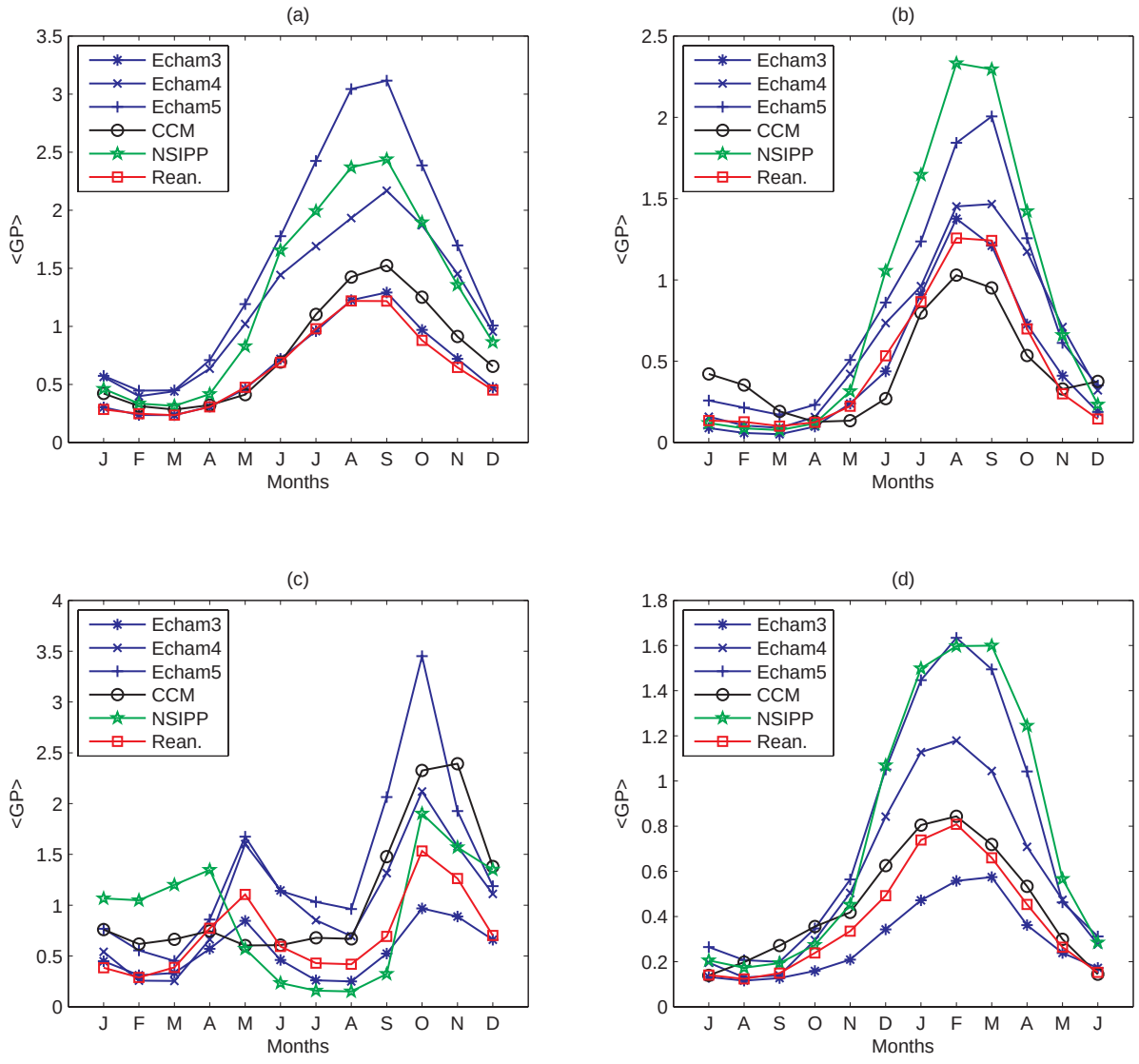

Figure 2: Annual cycle of mean genesis potential index in the models and reanalysis observations in the (a) Western North Pacific, (b) North Atlantic, (c) North Indian and (d) South Indian basins, in the period 1950-2004, with the exception the ECHAM5 model (for 1978-1999, resolution T42).

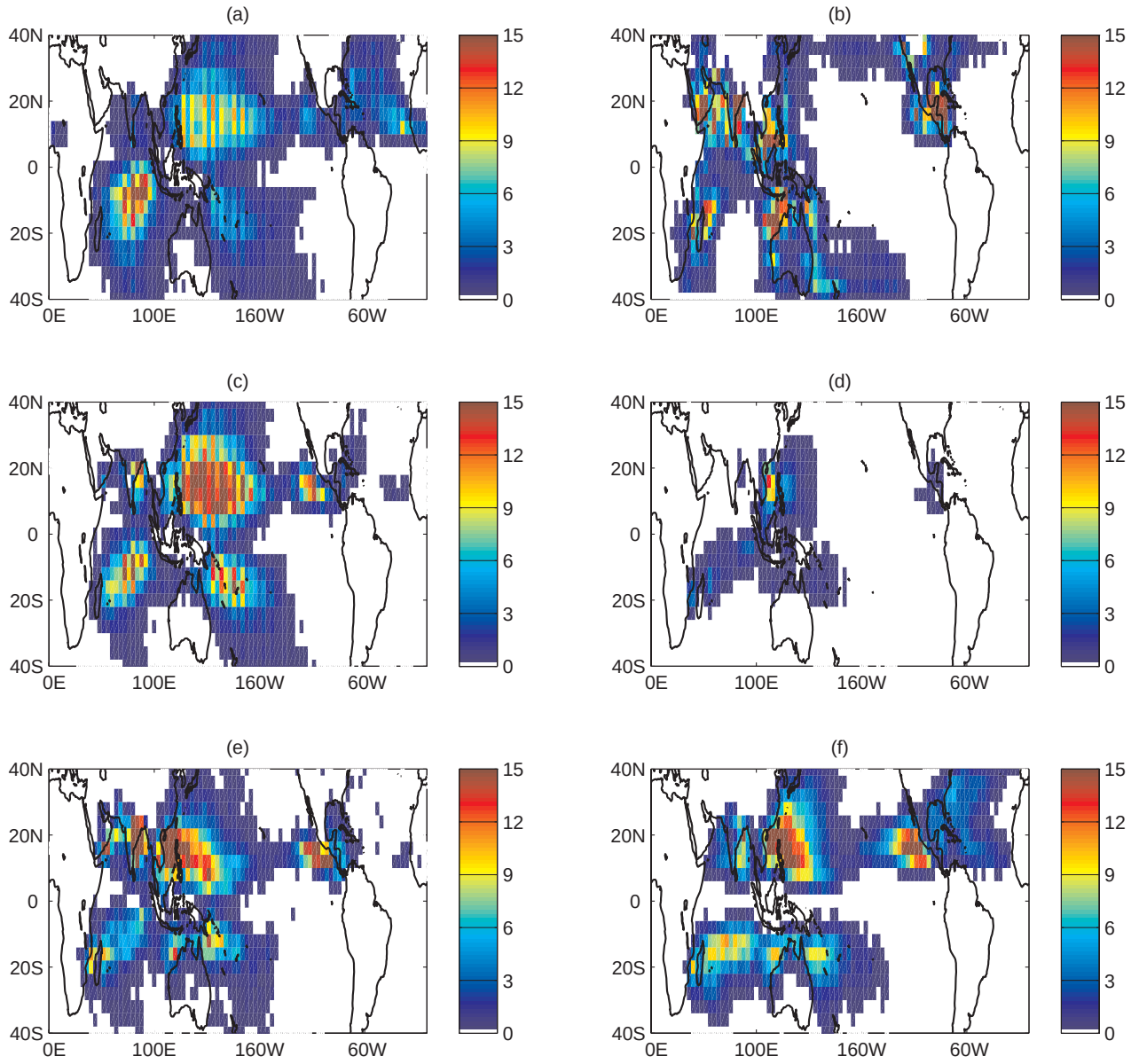

Figure 3: Track density climatological annual total in the period 1961-2000: (a) ECHAM3, (b) CCM3, (c) ECHAM4, (d) NSIPP, (e) ECHAM5 (for 1978-1999, resolution T42), (f) observations.

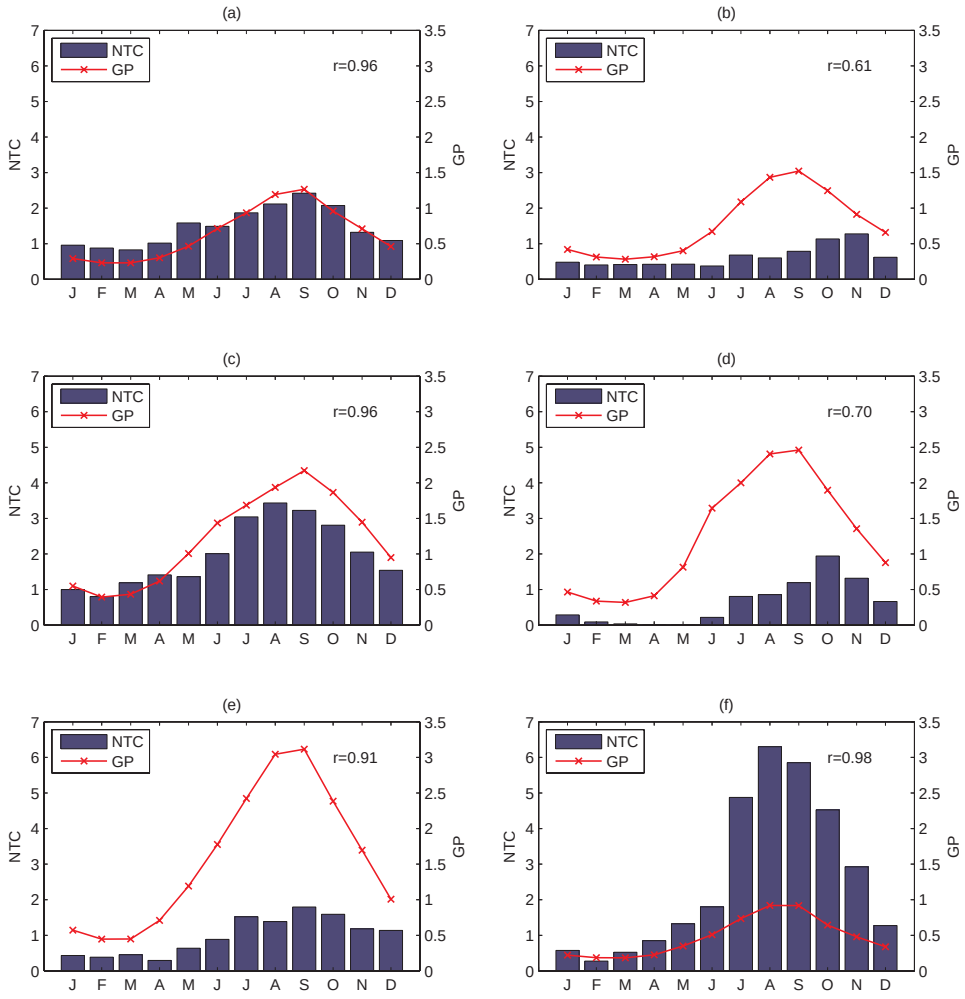

Figure 4: Annual cycle of genesis potential (GP) index (blue bars - left scale), and number of tropical cyclones (NTC) in the western North Pacific for the period 1961-2000 in models: ECHAM3 (a), CCM3 (b), ECHAM4 (c), NSIPP (d), ECHAM5 (for 1978-1999, resolution T42) (e), NCEP reanalysis GP and observed NTC (f).

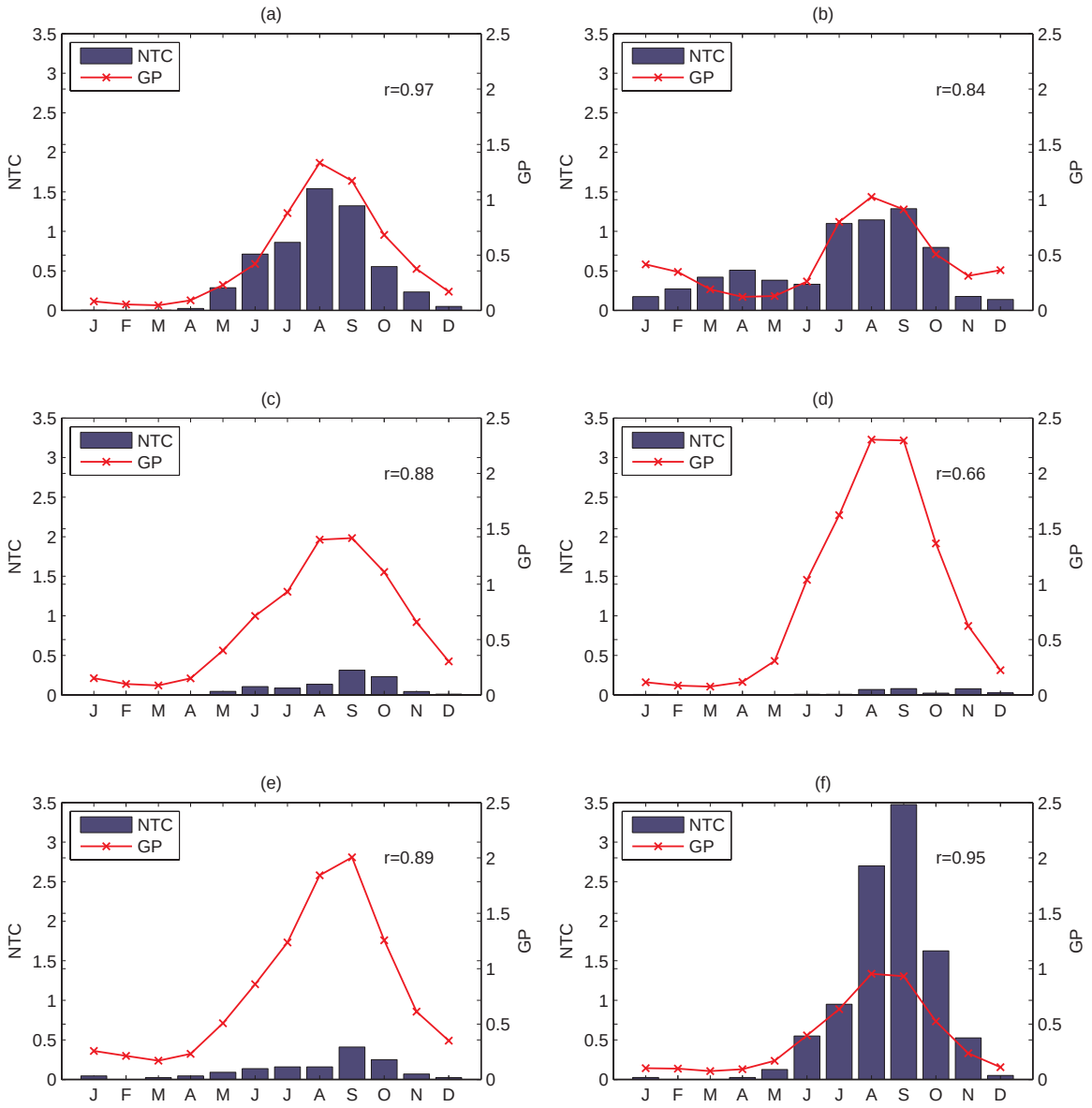

Figure 5: Annual cycle of genesis potential index (GPI) (blue bars - left scale), and number of tropical cyclones (NTC) in the w North Atlantic for the period 1961-2000 in models: ECHAM3 (a), CCM3 (b), ECHAM4 (c), NSIPP (d), ECHAM5 (for 1978-1999, resolution T42) (e), NCEP reanalysis GP and observed NTC (f).

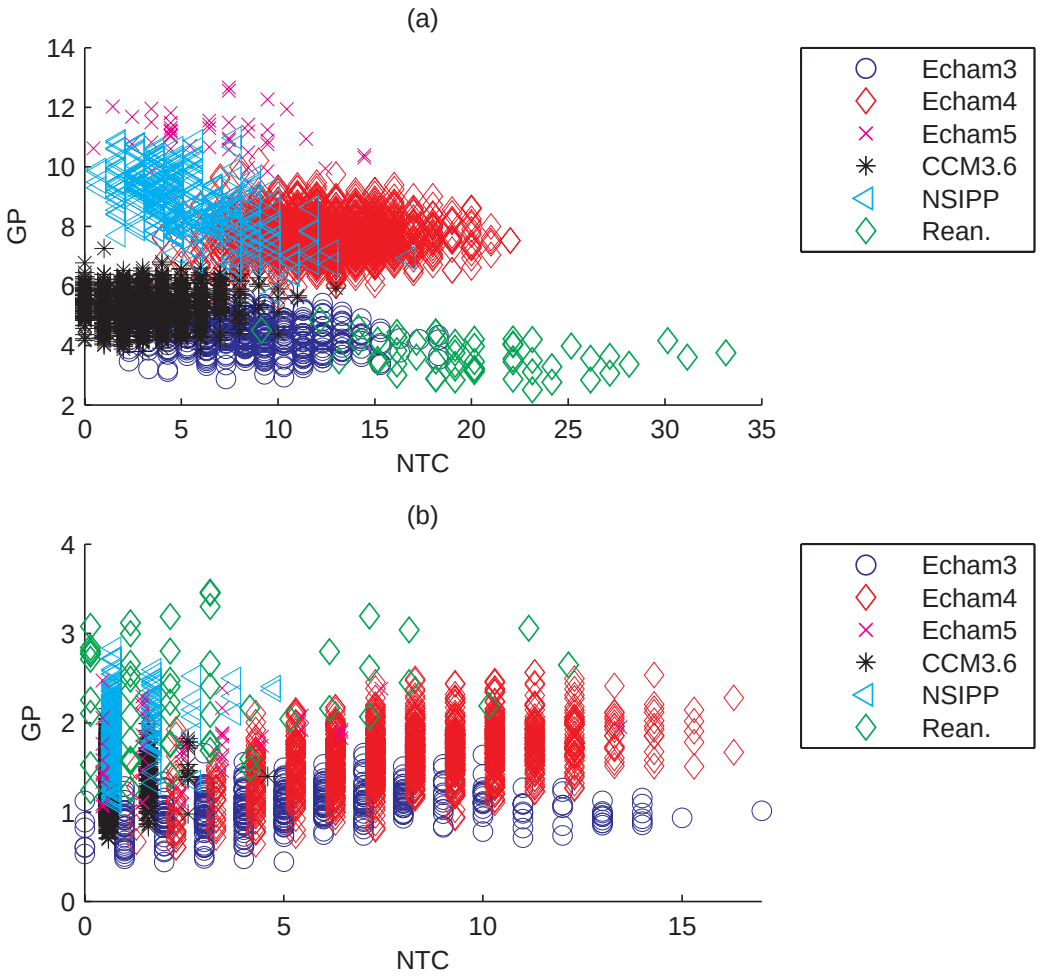

Figure 6: Scatter plot of number of model tropical cyclones (NTC) and genesis potential index (GPI) in the western North Pacific (a) and the eastern part of the western North Pacific (b)in the period July to October.

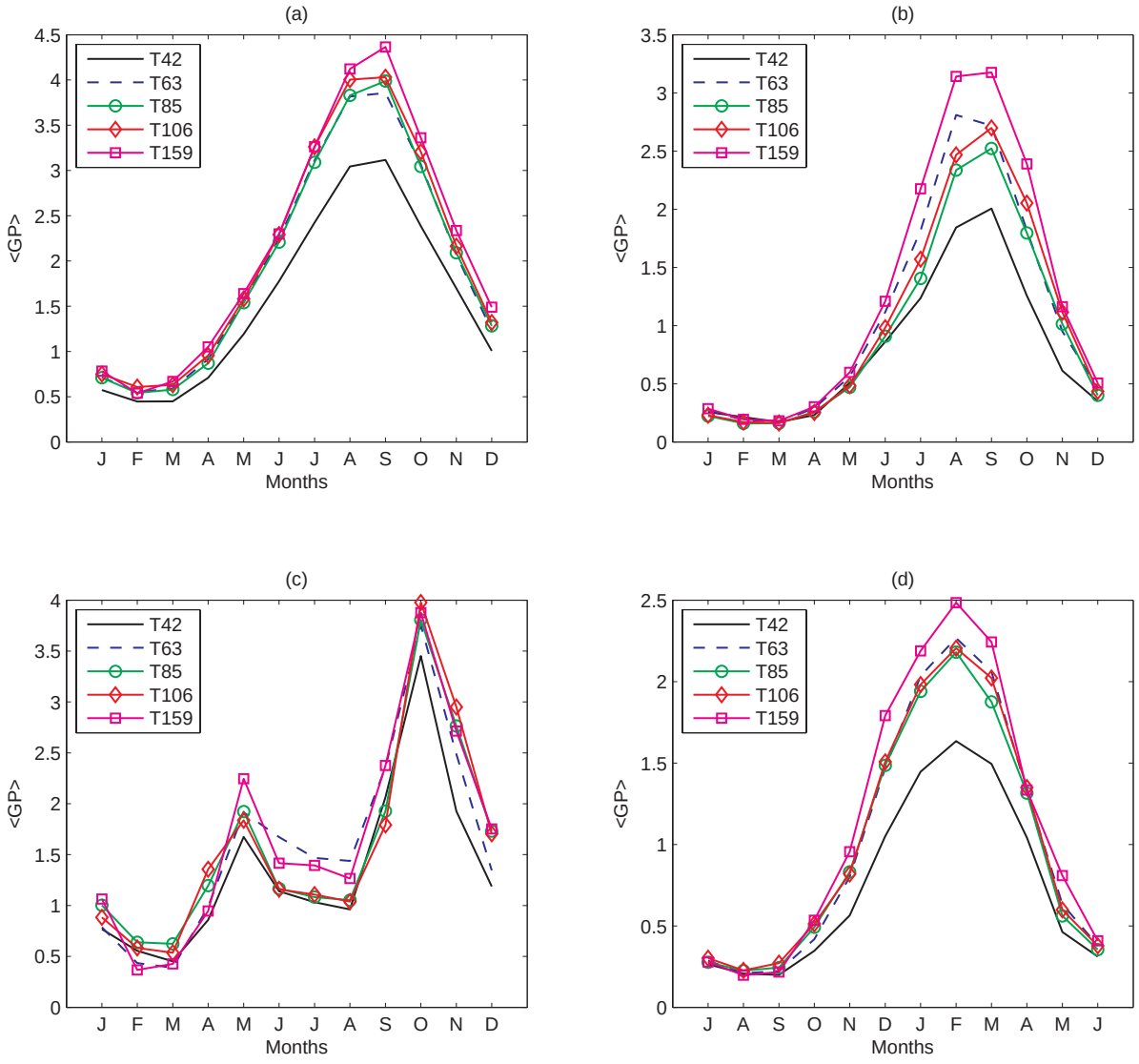

Figure 7: Genesis potential index in the period 1978-1999 for the ECHAM5 model for 5 different horizontal resolutions (T42, T63, T85, T106 and T159) in the (a) Western North Pacific, (b) North Atlantic, (c) North Indian and (d) South Indian basins.

List of Tables

1 Simulation properties of the models, including simulation period, horizontal (hor.) and vertical (vert.) resolutions, model type, number of ensemble members (ens.)and output type. ECHAM4 and NSIPP have different periods for the genesis potential (GP) and model tropical cyclones (TCs) analysis. 43

2 Definition of the regions of each basin and subbasin used in this study, as well as their peak seasons (JFM: January to March, DJF: December to February, OND: October to December, JASO: July to October, JAS: July to September and ASO: August to October) and acronyms. 44

3 Interannual correlations of the seasonal mean GPI, per basin (as defined in Table 2), between the models and the reanalysis for the peak TC season for the period 1950-2000 (ECHAM3), 1950-2004 (ECHAM4 and NSIPP), 1978-1999 (ECHAM5 - resolution T42), and 1950-2001 (CCM). Bold entries indicate correlation values that have significance at the 95% confidence level. 45

4 Interannual correlations of the seasonal mean GPI, per subbasin (as defined in Table 2), between the models and the reanalysis for the peak TC season for the period 1950-2000 (ECHAM3), 1950-2004 (ECHAM4 and NSIPP), 1978-1999 (ECHAM5 - resolution T42), and 1950-2001 (CCM). Bold entries indicate correlation values that have significance at the 95% confidence level. 46

5 Correlation between the model mean GPI, per basin (as defined in Table 2), and the total models' NTC in their peak TC season for the period 1950-2000 (ECHAM3), 1950-2004 (ECHAM4 and NSIPP), 1978-1999 (ECHAM5 - resolution T42), and 1950-2001 (CCM). Bold entries indicate correlation values that have significance at the 95% confidence level. Entries with an asterisk (∗) have zero model NTC counts for at least half of the years in the sample. 47

6 Correlation between the model mean GPI per subbasin (as defined in Table 2), and the total models' NTC in their peak TC season in the period 1950-2000 (ECHAM3), 1950-2004 (ECHAM4 and NSIPP), 1978-1999 (ECHAM5 - resolution T42), and 1950-2001 (CCM). Bold entries indicate correlation values that have significance at the 95% confidence level. Entries with an asterisk (∗) have zero model NTC counts for at least half of the years in the sample. 48

7 Correlation between the model mean GPI, per basin (as defined in Table 2), and the total NTC per basin in the observations for different basins in their peak TC season. Due to issues in data quality in the observations, the correlation was calculated for the period of 1971 onwards: 1971-2000 (ECHAM3), 1971-2004 (NCEP reanalysis, ECHAM4 and NSIPP), 1978-1999 (ECHAM5 - resolution T42), and 1971-2001 (CCM). Bold entries indicate correlation values that have significance at the 95% confidence level. Entries with an asterisk (∗) have zero model NTC counts for at least half of the years in the sample. 49

8 Correlation between the model mean GPI per subbasin (as defined in Table 2), and the total NTC per subbasin in the observations for in their peak TC season. Due to issues in data quality in the observations, the correlation was calculated for the period of 1971 onwards: 1971-2000 (ECHAM3), 1971-2004 (NCEP reanalysis, ECHAM4 and NSIPP), 1978-1999 (ECHAM5 - resolution T42), and 1971-2001 (CCM). Bold entries indicate correlation values that have significance at the 95% confidence level. Entries with an asterisk (∗) have zero model NTC counts for at least half of the years in the sample. 50

Table 1: Simulation properties of the models, including simulation period, horizontal (hor.) and vertical (vert.) resolutions, model type, number of ensemble members (ens.)and output type. ECHAM4 and NSIPP have different periods for the genesis potential (GP) and model tropical cyclones (TCs) analysis.

Model	Years	Hor. Res.	Vert. Res.	Type	Ens.	Output type
ECHAM3	1950-2000	T42	L19	spectral	10	6 hourly, Monthly
ECHAM4 (GP)	1950-2004	T42	L19	spectral	24	Monthly
ECHAM4 (TCs)	1950-2002	T42	L19	spectral	24	6 hourly
ECHAM5	1978-1999	T42	L19, L31	spectral	2	6 hourly, Monthly
ECHAM5	1978-1999	T63	L19, L31	spectral	5	6 hourly, Monthly
ECHAM5	1978-1999	T85	L19, L31	spectral	2	6 hourly, Monthly
ECHAM5	1978-1999	T106	L19, L31	spectral	2	6 hourly, Monthly
ECHAM5	1978-1999	T159	L31	spectral	1	6 hourly, Monthly
CCM	1950-2001	T42	L19	spectral	24	Daily, Monthly
NSIPP (GP)	1950-2004	$2.5^\circ \times 2^\circ$	L34	grid point	9	Monthly
NSIPP (TCs)	1961-2000	$2.5^\circ \times 2^\circ$	L34	grid point	9	Daily

Table 2: Definition of the regions of each basin and subbasin used in this study, as well as their peak seasons (JFM: January to March, DJF: December to February, OND: October to December, JASO: July to October, JAS: July to September and ASO: August to October) and acronyms.

Region	Acronym	Latitudes	Longitudes	Peak season
South Indian	SI	40°S - 0°	30°E - 100°E	JFM
S. Indian South	SI S	40°S - 10°	30°E - 100°E	JFM
S. Indian North	SI N	10°S - 0°	30°E - 100°E	JFM
Australian	AUS	40°S - 0°	100°E - 180°	JFM
Australian South	AUS S	40°S - 10°	100°E - 180°	JFM
Australian North	AUS N	10°S - 0°	100°E - 180°	JFM
South Pacific	SP	40°S - 0°	180° - 110°W	DJF
S. Pacific South	SP S	40°S - 10°	180° - 110°W	DJF
S. Pacific North	SP N	10°S - 0°	180° - 110°W	DJF
North Indian	NI	0° - 30°N	40°E - 100°E	OND
North Indian West	NI W	0° - 30°N	40°E - 77°E	OND
North Indian East	NI E	0° - 30°N	77°E - 100°E	OND
Western North Pacific	WNP	0° - 40°N	100°E - 165°W	JASO
W. North Pacific East	WNP E	0° - 40°N	100°E - 135°E	JASO
W. North Pacific West	WNP W	0° - 40°N	135°E - 165°W	JASO
Eastern North Pacific	ENP	0° - 40°N	135°E to American coast	JAS
North Atlantic	ATL	0° - 40°N	American to African coast	ASO
N. Atlantic West	ATL W	0° - 25°N	American coast to 30°W	ASO
N. Atlantic East	ATL E	0° - 25°N	30°W to African coast	ASO

Table 3: Interannual correlations of the seasonal mean GPI, per basin (as defined in Table 2), between the models and the reanalysis for the peak TC season for the period 1950-2000 (ECHAM3), 1950-2004 (ECHAM4 and NSIPP), 1978-1999 (ECHAM5 - resolution T42), and 1950-2001 (CCM). Bold entries indicate correlation values that have significance at the 95% confidence level.

Model	Resol	SI	AUS	SP	NI	WNP	ENP	ATL
CCM	T42	-0.19	**0.51**	-0.10	**0.28**	-0.13	**0.57**	**0.58**
NSIPP	2.5°	-0.31	0.19	0.04	**0.28**	**0.29**	**0.60**	**0.38**
ECHAM3	T42	0.08	**0.37**	0.20	**0.35**	**0.45**	**0.41**	**0.59**
ECHAM4	T42	0.05	**0.49**	0.21	0.20	0.21	**0.44**	**0.74**
ECHAM5	T42	-0.04	0.30	0.03	-0.09	**0.46**	**0.52**	**0.48**
ECHAM5	T63	0.02	**0.50**	0.03	0.31	**0.50**	0.37	0.41
ECHAM5	T85	-0.02	0.34	-0.01	0.41	**0.52**	0.38	**0.52**
ECHAM5	T106	0.08	0.41	0.01	0.34	0.33	**0.58**	0.37
ECHAM5	T159	0.10	**0.48**	0.33	**0.64**	0.27	0.35	0.37

Table 4: Interannual correlations of the seasonal mean GPI, per subbasin (as defined in Table 2), between the models and the reanalysis for the peak TC season for the period 1950-2000 (ECHAM3), 1950-2004 (ECHAM4 and NSIPP), 1978-1999 (ECHAM5 - resolution T42), and 1950-2001 (CCM). Bold entries indicate correlation values that have significance at the 95% confidence level.

Model	Resol	SI S	SI N	AUS S	AUS N	SP S	SP N
CCM	T42	-0.02	**0.36**	**0.67**	**0.34**	**0.29**	**0.74**
NSIPP	2.5°	-0.20	**0.33**	**0.55**	**0.35**	**0.37**	**0.75**
ECHAM3	T42	0.23	0.11	**0.58**	0.27	**0.46**	**0.78**
ECHAM4	T42	0.18	**0.34**	**0.65**	**0.36**	**0.47**	**0.85**
ECHAM5	T42	-0.16	**0.57**	0.42	0.40	0.42	**0.92**
ECHAM5	T63	-0.19	**0.49**	**0.62**	**0.60**	**0.45**	**0.91**
ECHAM5	T85	-0.20	0.16	**0.51**	0.19	0.39	**0.93**
ECHAM5	T106	-0.05	0.38	**0.61**	**0.52**	0.40	**0.89**
ECHAM5	T159	-0.03	**0.48**	**0.64**	**0.47**	**0.50**	**0.93**
Model	Resol	NI W	NI E	WNP W	WNP E	ATL W	ATL E
CCM	T42	**0.50**	0.03	-0.19	**0.50**	**0.75**	-0.08
NSIPP	2.5°	**0.29**	0.20	**0.51**	**0.63**	**0.48**	-0.15
ECHAM3	T42	**0.58**	0.19	**0.63**	**0.64**	**0.67**	-0.08
ECHAM4	T42	**0.38**	0.18	**0.54**	**0.59**	**0.79**	-0.07
ECHAM5	T42	0.04	-0.07	**0.73**	**0.71**	**0.66**	0.12
ECHAM5	T63	0.36	0.24	**0.73**	**0.69**	**0.63**	0.01
ECHAM5	T85	0.36	0.15	**0.74**	**0.67**	**0.65**	0.07
ECHAM5	T106	0.08	0.40	**0.67**	**0.52**	**0.54**	0.23
ECHAM5	T159	**0.48**	**0.46**	**0.45**	**0.71**	**0.55**	0.28

Table 5: Correlation between the model mean GPI, per basin (as defined in Table 2), and the total models' NTC in their peak TC season for the period 1950-2000 (ECHAM3), 1950-2004 (ECHAM4 and NSIPP), 1978-1999 (ECHAM5 - resolution T42), and 1950-2001 (CCM). Bold entries indicate correlation values that have significance at the 95% confidence level. Entries with an asterisk ($*$) have zero model NTC counts for at least half of the years in the sample.

Model	SI	AUS	SP	NI	WNP	ENP	ATL
CCM	**0.40**	**0.28**	**0.48**	**0.71**	0.09	-0.20	-0.01
NSIPP	**0.55**	**0.49**	0.26	0.16$*$	-0.76	-0.33	-0.05
ECHAM3	**0.40**	-0.45	-0.27	0.22	-0.21	**0.66**	**0.41**
ECHAM4	**0.47**	0.12	-0.28	0.21	**0.40**	**0.59**	**0.77**
ECHAM5	0.11	-0.18	-0.15	0.36	0.08	0.13	0.15

Table 6: Correlation between the model mean GPI per subbasin (as defined in Table 2), and the total models' NTC in their peak TC season in the period 1950-2000 (ECHAM3), 1950-2004 (ECHAM4 and NSIPP), 1978-1999 (ECHAM5 - resolution T42), and 1950-2001 (CCM). Bold entries indicate correlation values that have significance at the 95% confidence level. Entries with an asterisk ($*$) have zero model NTC counts for at least half of the years in the sample.

Model	SI S	SI N	AUS S	AUS N	SP S	SP N
CCM	**0.56**	-0.10	**0.36**	-0.30	**0.52**	0.06$*$
NSIPP	**0.58**	**0.34**	**0.54**	0.18	0.18	**0.79**$*$
ECHAM3	0.27	**0.53**	0.11	**0.67**	-0.11	**0.92**$*$
ECHAM4	**0.46**	**0.61**	**0.69**	**0.32**	**0.42**	**0.95**
ECHAM5	-0.05	0.32	**0.47**	0.39	0.32$*$	**0.92**$*$
Model	NI W	NI E	WNP W	WNP E	ATL W	ATL E
CCM	**0.63**	**0.74**	**0.30**	0.19	0.26	0.01$*$
NSIPP	-0.32$*$	0.31$*$	-0.81	**0.55**	0.17	0.00$*$
ECHAM3	0.06$*$	**0.40**	-0.01	**0.33**	**0.60**	**0.84**
ECHAM4	0.16	0.22	**0.61**	**0.84**	**0.84**	**0.44**
ECHAM5	-0.02$*$	0.39$*$	-0.07	**0.46**	0.25	0.09$*$

Table 7: Correlation between the model mean GPI, per basin (as defined in Table 2), and the total NTC per basin in the observations for different basins in their peak TC season. Due to issues in data quality in the observations, the correlation was calculated for the period of 1971 onwards: 1971-2000 (ECHAM3), 1971-2004 (NCEP reanalysis, ECHAM4 and NSIPP), 1978-1999 (ECHAM5 - resolution T42), and 1971-2001 (CCM). Bold entries indicate correlation values that have significance at the 95% confidence level. Entries with an asterisk ($*$) have zero model NTC counts for at least half of the years in the sample.

Model	Resol	SI	AUS	SP	NI	WNP	ENP	ATL
reanalysis	2.5°	0.23	0.25	**0.38**	0.06	0.13	0.22	**0.60**
CCM	T42	-0.29	**0.46**	-0.28	-0.10	0.30	0.30	**0.46**
NSIPP	2.5°	-0.09	0.31	-0.09	0.27	0.10	0.29	**0.50**
ECHAM3	T42	-0.01	**0.50**	-0.29	0.10	-0.20	0.17	0.00
ECHAM4	T42	0.09	**0.37**	-0.27	**0.35**	0.17	0.28	**0.36**
ECHAM5	T42	-0.02	0.29	-0.09	-0.01	0.21	**0.56**	**0.53**
ECHAM5	T63	-0.06	0.39	-0.05	-0.05	0.21	**0.54**	0.33
ECHAM5	T85	-0.09	0.20	-0.03	0.01	0.28	**0.47**	**0.47**
ECHAM5	T106	-0.01	0.30	-0.13	0.11	-0.04	**0.62**	0.27
ECHAM5	T159	0.05	0.38	0.30	0.01	0.21	**0.54**	**0.43**

Table 8: Correlation between the model mean GPI per subbasin (as defined in Table 2), and the total NTC per subbasin in the observations for in their peak TC season. Due to issues in data quality in the observations, the correlation was calculated for the period of 1971 onwards: 1971-2000 (ECHAM3), 1971-2004 (NCEP reanalysis, ECHAM4 and NSIPP), 1978-1999 (ECHAM5 - resolution T42), and 1971-2001 (CCM). Bold entries indicate correlation values that have significance at the 95% confidence level. Entries with an asterisk ($*$) have zero model NTC counts for at least half of the years in the sample.

Model	SI S	SI N	AUS S	AUS N	SP S	SP N
reanalysis	**0.43**	0.07	**0.37**	0.16	0.19	**0.77**
CCM	0.02	-0.03	**0.57**	0.30	-0.09	**0.66**$*$
NSIPP	-0.19	0.26	**0.50**	0.24	-0.02	**0.70**$*$
ECHAM3	0.07	0.12	**0.69**	0.17	-0.18	**0.64**$*$
ECHAM4	0.19	0.19	**0.53**	0.25	-0.09	**0.74**$*$
ECHAM5	-0.03	-0.08	**0.48**	0.07	-0.06	**0.77**$*$
Model	NI W	NI E	WNP W	WNP E	ATL W	ATL E
reanalysis	0.18	0.12	0.31	**0.67**	**0.67**	0.11
CCM	-0.14	-0.04	-0.01	**0.47**	**0.60**	0.10
NSIPP	-0.21	**0.38**	0.26	**0.73**	**0.52**	0.21
ECHAM3	-0.02	0.12	0.34	0.18	0.18	-0.23
ECHAM4	0.05	**0.39**	**0.43**	**0.49**	**0.49**	0.04
ECHAM5	0.13	0.04	**0.51**	**0.55**	**0.58**	0.06